Heavy quarkonium production: Nontrivial transition from pA to AA collisions

B. Z. Kopeliovich,[1,2] I. K. Potashnikova,[1] H. J. Pirner,[2] and Iván Schmidt[1]

[1]*Departamento de Física Universidad Técnica Federico Santa María, Instituto de Estudios Avanzados en Ciencias e Ingeniería, and Centro Científico–Tecnológico de Valparaíso, Casilla 110-V, Valparaíso, Chile*

[2]*Institut für Theoretische Physik der Universität, Philosophenweg 19, D-69120 Heidelberg, Germany*

(Received 26 August 2010; published 28 January 2011)

Two novel QCD effects, double-color filtering and mutual boosting of the saturation scales in colliding nuclei, affect the transparency of the nuclei for quark dipoles in comparison with proton-nucleus collisions. The former effect increases the survival probability of the dipoles, since color filtering in one nucleus makes the other one more transparent. The second effect acts in the opposite direction and is stronger; it makes the colliding nuclei more opaque than in the case of pA collisions. As a result of parton saturation in nuclei the effective scale is shifted upward, which leads to an increase of the gluon density at small x. This in turn leads to a stronger transverse momentum broadening in AA compared with pA collisions, i.e., to an additional growth of the saturation momentum. Such a mutual boosting leads to a system of reciprocity equations, which result in a saturation scale, a few times higher in AA than in pA collisions at the energies of the large hadron collider (LHC). Since the dipole cross section is proportional to the saturation momentum squared, the nuclei become much more opaque for dipoles in AA than in pA collisions. For the same reason gluon shadowing turns out to be boosted to a larger magnitude compared with the product of the gluon shadowing factors in each of the colliding nuclei. All these effects make it more difficult to establish a baseline for anomalous J/Ψ suppression in heavy ion collisions at high energies.

DOI: 10.1103/PhysRevC.83.014912 PACS number(s): 24.85.+p, 25.75.Bh, 25.75.Cj, 14.40.Pq

I. INTRODUCTION

Nuclear suppression of heavy quarkonia is usually considered as a sensitive hard probe for the properties of the short-living medium produced in Heavy ions collisions [1–3]. The main challenge is to discriminate between initial state interactions (ISI), usually identified as cold nuclear matter effects, and final state interaction (FSI), which is related to attenuation of the produced quarkonium in the dense matter created in the nuclear collision. While the latter is the main goal of the study, experimental information fully depends on how well we understand the ISI contribution.

Naturally the ISI dynamics should be studied in a proton-nucleus collision, where no dense matter is expected to be produced. The next step, the extrapolation of the results to nuclear collisions, is not that easy. Usually it is done in an oversimplified manner, assuming that a $\bar{c}c$ pair is produced momentarily inside the nucleus and then attenuates with an unknown absorption cross section on the way out of the nucleus. The $\bar{c}c$ breakup cross section is fitted to pA data and used to predict the ISI effects in AA collisions. As we will show, the breakup cross section is not constant but steeply rises with the $\bar{c}c$ energy; in addition, it is well known from Hadron Elektron Ring Anlage (HERA) data. The most appealing oversimplification, especially at the high energies of the relativistic heavy ion collider (RHIC) and large hadron collider (LHC), is the instantaneous production of $\bar{c}c$. In reality the production time ranges from tens to thousands of fermis at these energies. The long production time leads to shadowing, which is a high-twist effect suppressed by the quark mass squared. Nevertheless, we find that this shadowing effect is stronger than the leading twist gluon shadowing, which produces a rather mild suppression even at the LHC in the central rapidity region.

Even if the shadowing and breakup effects in pA collisions are under control, one still cannot predict the cold nuclear effects in AA collisions in a model-independent way. The two major phenomena considered in this paper make this impossible. The first one is double-color filtering of dipoles propagating simultaneously through two nuclei. As we will demonstrate, the survival probability of a dipole in AA collisions is higher than the product of that in each of the colliding nuclei.

Another effect changing the properties of the cold nuclear medium in AA collisions is the boosting of the saturation scales in the nuclei due to mutual multiple interactions in the nuclei. The effect is especially strong at the energies of the LHC. The nuclear medium becomes several times more opaque for dipoles compared with its transparency in pA collisions. These two effects essentially modify the effects of the ISI stage of heavy ion collisions, which is usually considered to be the baseline for search for "anomalous" nuclear suppression of heavy quarkonia.

All calculations in this paper are performed in so called frozen approximation, neglecting the size fluctuations of dipoles during their propagation through nuclei. This approximation is accurate provided that the coherence length for heavy quark production substantially exceeds the size of the nuclei. This condition is satisfied at the energies of the RHIC and above.

II. PROTON-NUCLEUS COLLISIONS

First, one should make sure that the nuclear effects for heavy quarkonium production in pA collisions are understood, as well as the absolute magnitude of the cross section. The cross sections of χ and J/Ψ production in pp collisions were successfully reproduced in the color-singlet model in Refs. [4] and [5], respectively. What has been missed in most of current analyses of J/Ψ production in pA collisions are the coherence effects related to the long timescale of charm production,

associated with propagation of a color-octet $\bar{c}c$ pair through the nucleus prior the production of a colorless dipole [4,6]. This stage results in the heavy quark shadowing, which is of the same order as the effect of breakup of the colorless dipole. Although both are the high-twist effects, quantitatively they are more important for currently available data than the suppression caused by the leading twist gluon shadowing. The latter is frequently miscalculated being based on some nuclear gluon parton distribution function parton distribution function (PDFs), which rely on either ad hoc or incorrect assumptions (see discussion in Ref. [3]).

A. High-twist heavy quark shadowing

Although the proper time of charm production is short, $t_c^* \sim 1/(2m_c)$, this time rises with J/Ψ energy linearly in the rest frame of the nucleus,

$$t_c \sim \frac{2E}{M^2_{J/\Psi}}. \tag{1}$$

Thus, if the energy of the produced J/Ψ is sufficiently high, $E \gtrsim 25(\,\mathrm{GeV}) \times L(\,\mathrm{fm})$, effects of coherence become significant. At the energy of the RHIC, $\sqrt{s} = 200\,\mathrm{GeV}$, and positive rapidities, $t_c > 12\,\mathrm{fm}$. For Υ production t_c at the RHIC is rather short but becomes much longer than the nuclear size at the energies of the LHC. In what follows we assume the coherence time to be much longer than the nuclear size, unless otherwise specified.

The nuclear suppression caused by coherence can be interpreted as high-twist shadowing in the process of $\bar{c}c$ pair production by a projectile gluon. The $\bar{c}c$ is produced coherently in multiple interactions of the projectile gluon with target nucleons. If the J/Ψ energy is sufficiently high, so that $t_c \gg R_A$, one can neglect the dipole size fluctuations during propagation through the nucleus; i.e., we treat the dipoles being "frozen" by Lorentz time dilation.

Since the production amplitude is convoluted with the charmonium wavefunction, one can assume with good accuracy an equal sharing of the total longitudinal momentum between c and $\bar{c}$. In what follows we rely on the saturated parametrization of the dipole cross section [7]

$$\sigma_{\bar{c}c}(r_T, x_2) = \sigma_0\big(1 - e^{-r_T^2/r_0^2(x_2)}\big), \tag{2}$$

where $\sigma_0 = 23.03\,\mathrm{mb}$, $r_0(x_2) = 0.4\,\mathrm{fm} \times (x_2/x_0)^{0.144}$, $x_0 = 3.04 \times 10^{-4}$; $x_2 = e^{-y}\sqrt{\langle M^2_{\bar{c}c}\rangle + \langle p_T^2\rangle}/\sqrt{s}$. The $\bar{c}c$ invariant mass distribution predicted by the color-singlet model leads to $\langle M^2_{\bar{c}c}\rangle = 2M^2_{J/\Psi}$ [2]. The measured $\langle p_T^2\rangle = 4\,\mathrm{GeV}^2$.

The amplitude of $\bar{c}c$ production at a point with impact parameter b and longitudinal coordinate z inside the nucleus, averaged over the dipole size reads [4]

$$S_{pA}(b,z) = \int d^2r_T\, W_{\bar{c}c}(r_T) \times \exp\left[-\frac{1}{2}\sigma_{\bar{c}cg}(r_T)T_-(b,z) - \frac{1}{2}\sigma_{\bar{c}c}(r_T)T_+(b,z)\right]. \tag{3}$$

Here $T_-(b,z) = \int_{-\infty}^{z} dz'\rho_A(b,z')$, $T_+(b,z) = T_A(b) - T_-(b,z)$, and $T_A(b) = T_-(b,\infty)$. According to Ref. [4] shadowing for $\bar{c}c$ production over the nuclear thickness $T_-(b,z)$ occurs with the shadowing cross section corresponding to a three-body dipole, gluon, and $\bar{c}c$, which for equal momenta of c and $\bar{c}$ equals to $\sigma_{\bar{c}cg}(r_T) = \frac{9}{4}\sigma_{\bar{c}c}(r_T/2) - \frac{1}{8}\sigma_{\bar{c}c}(r_T)$.

The survival probability amplitude (3) should be squared and integrated over the coordinate of the production point. Then the nuclear ratio reads

$$R_{pA} = \frac{1}{A}\int d^2b \int_{-\infty}^{\infty} dz\,|S_{pA}(b,z)|^2. \tag{4}$$

We rely on the form of nuclear effects for production of the P-wave charmonium χ_2 derived in Ref. [4]. The mechanism of J/Ψ production is more complicated, but the general structure of shadowing corrections should be similar because the overlap of the initial narrow size distribution of the perturbatively produced $\bar{c}c$ pair with the large-size wavefunction of the final charmonium is dominated by the small initial size $\sim 1/m_c$, whether the charmonium is χ or J/Ψ. In addition, χ decays contribute about 30% to J/Ψ production.

In the regime of long $t_c \gg R_A$, the weight factor in Eq. (3) has the form [4]

$$W_{\bar{c}c}(r_T) \propto K_0(m_c r_T)\, r_T^2\, \Psi_{J/\Psi}(r_T), \tag{5}$$

where one factor r_T comes from the amplitude of $\bar{c}c$ production, and another one either from the amplitude of gluon radiation in the case J/Ψ production or from the radial wave function of χ_2. Further, we assume the wavefunction to have the oscillatory form, $\Psi_{J/\Psi}(r_T) \propto \exp[-r_T^2/2\langle r^2_{J/\Psi}\rangle]$ with $\langle r^2_{J/\Psi}\rangle = 2/m_c\omega$, $m_c = 1.5\,\mathrm{GeV}$, and $\omega = 300\,\mathrm{MeV}$ [8].

To simplify the calculations we use for $\Psi^c_{\mathrm{in}}(r_T) = r_T^2\, K_0(r_T m_c)$ the parametrization proposed in Ref. [8],

$$\Psi^c_{in}(r_T) \approx \mathrm{const.} \times \left[e^{-r_T^2/a_c^2} - e^{-r_T^2/b_c^2}\right], \tag{6}$$

where $a_c = 0.496\,\mathrm{fm}$, $b_c = 0.11\,\mathrm{fm}$. The comparison of the two functions Eq. (6) plotted in Fig. 1 demonstrates that the approximation is rather accurate within the range of r_T we are interested in.

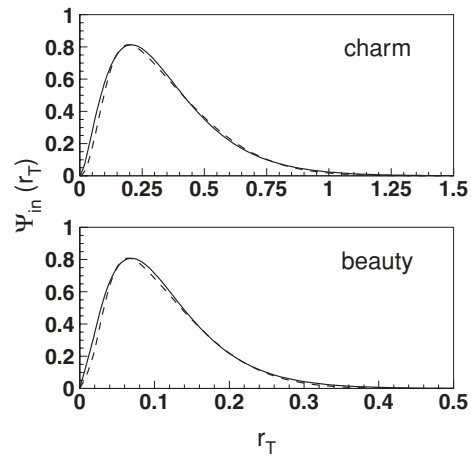

FIG. 1. Comparison of the left-hand (solid curves) and right-hand (dashed) sides of Eq. (6). The top and bottom panels are for charm and beauty, respectively.

Thus, we present the weight factor $W_{\bar{c}c}$ (5) in the form

$$W_{\bar{c}c}(r_T) = \frac{1}{\pi\left(r_1^2 - r_2^2\right)}\left(e^{-r_T^2/r_1^2} - e^{-r_T^2/r_2^2}\right), \tag{7}$$

where $r_1^2 = a_c^2/(1 + a_c^2/2\langle r_{J/\Psi}^2\rangle)$ and $r_2^2 = b_c^2/(1 + b_c^2/2\langle r_{J/\Psi}^2\rangle)$.

In a small-r_T approximation the dipole-nucleon cross sections in Eq. (3) have the simple form $\sigma_{\bar{c}c}(r_T, x_2) = C(x_2)\, r_T^2$ and $\sigma_{\bar{c}cg}(r_T, x_2) = \frac{7}{16} C(x_2)\, r_T^2$. So the integration can be performed analytically, and we arrive at

$$S_{pA}(b) = \frac{1}{r_1^2 - r_2^2}\left[r_1^2\, S_{pA}^{(1)}(b) - r_2^2\, S_{pA}^{(2)}(b)\right], \tag{8}$$

where for $i = 1, 2$,

$$S_{pA}^{(i)}(b) = \left\{1 + \tfrac{1}{2} C\, r_i^2 \left[\tfrac{7}{16} T_-(b, z) + T_+(b, z)\right]\right\}^{-1}. \tag{9}$$

Notice that due to color transparency the nuclear medium is more transparent than in the Glauber model. Moreover, the amplitude (9) does not decrease with nuclear thickness exponentially, but as a power.

Finally, we integrate the attenuation factor (8) squared over the coordinates of the production point and arrive at the nuclear ratio, which has the form

$$R_{pA} = \left(\frac{r_1^2}{r_1^2 - r_2^2}\right)^2 R_{pA}^{(1)} + \left(\frac{r_2^2}{r_1^2 - r_2^2}\right)^2 R_{pA}^{(2)} - 2\left(\frac{r_1 r_2}{r_1^2 - r_2^2}\right)^2 R_{pA}^{(12)}, \tag{10}$$

where for $i = 1, 2$,

$$R_{pA}^{(i)} = \frac{1}{A}\int d^2b\, T_A(b)\left[1 + \frac{r_i^2}{2}\, C\, T_A(b)\right]^{-1} \times \left[1 + \frac{7 r_i^2}{32}\, C\, T_A(b)\right]^{-1}, \tag{11}$$

and

$$R_{pA}^{(12)} = \frac{1}{A}\,\frac{32}{9C\left(r_1^2 - r_2^2\right)}\int d^2b \times \ln\left\{\frac{\left[1 + \frac{r_1^2}{2} C\, T_A(b)\right]\left[1 + \frac{7r_2^2}{32} C\, T_A(b)\right]}{\left[1 + \frac{r_2^2}{2} C\, T_A(b)\right]\left[1 + \frac{7r_1^2}{32} C\, T_A(b)\right]}\right\}. \tag{12}$$

With these equations we calculated the nuclear ratio $R_{A/p}(y)$, Eq. (10). We rely on the realistic Woods-Saxon parametrization for the nuclear density [9]. The results at $\sqrt{s} = 200$ GeV are depicted as function of rapidity in Fig. 2 by dotted curve.

We see that the steep rise of the breakup cross section $\sigma_{\bar{c}c}(r_T, E_{\bar{c}c})$ with energy (it triples from $y = 0$ to $y = 2$) explains well the observed rapidity dependence of nuclear suppression. The calculations should not be continued far to negative rapidities, since the regime of long coherence length breaks down there. In addition, additional mechanisms, which cause a nuclear enhancement at negative rapidities, must be added.

We also tested how accurate is the result of analytic integration (10) and performed numerical calculation using the full equation (3) with the dipole cross section (2). The results is plotted by dashed curve in Fig. 2. It is pretty close to the previously calculated dotted curve. Both agree with data within large errors and normalization uncertainty.

In Fig. 3 we present the impact parameter dependence of nuclear suppression for J/Ψ produced with different rapidities in p-Au collisions at the RHIC. As expected, the strongest dependence on rapidity comes from most central collisions.

We also performed calculations for nuclear effects in Υ production. The only difference with charmonium production is the heavier quark mass, $m_b = 4.5$ GeV, and new values of parameters in the parametrization (6), $a_b = 0.162$, $b_b = 0.037$. How accurate is this parametrization for bottom quarks is demonstrated in the bottom panel of Fig. 1. The results for nuclear suppression of Υ produced in lead at the energies of the RHIC, $\sqrt{s} = 200$ GeV, and the LHC, $\sqrt{s} = 5.5$ TeV, as function of rapidity are depicted in Fig. 4.

The upper solid and bottom dashed curves are calculated at $\sqrt{s} = 200$ GeV and 5.5 TeV, respectively. Notice that in the

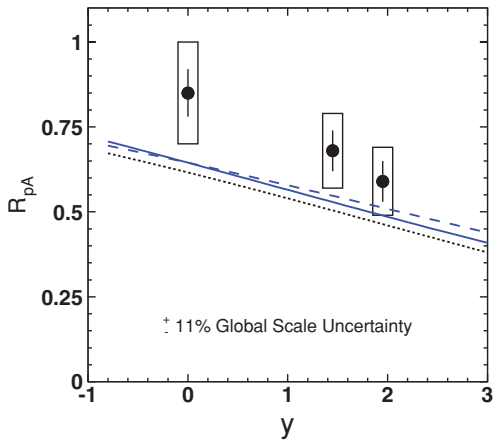

FIG. 2. (Color online) Dashed curve presents nuclear suppression of J/Ψ as function of rapidity in pA collisions. Solid curve is corrected for gluon shadowing. Data are for dAu collisions at $\sqrt{s} = 200$ GeV [10].

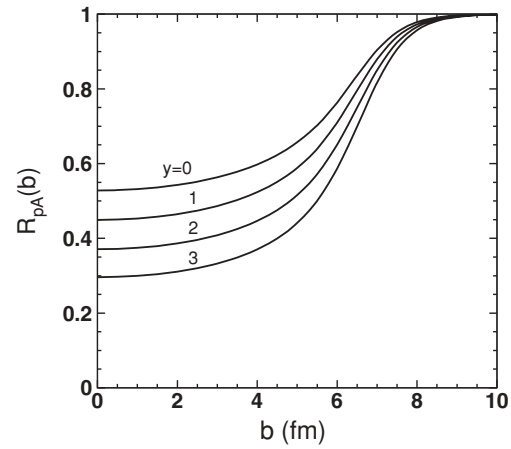

FIG. 3. b dependence of the nuclear ratios for J/Ψ produced with rapidities $y = 0,\ 1,\ 2,\ 3$ in pAu collisions at $\sqrt{s} = 200$ GeV.

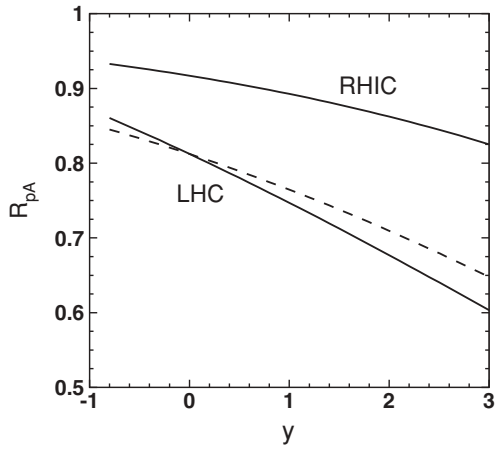

FIG. 4. Nuclear suppression of Υ production as function of rapidity in pA collisions at $\sqrt{s} = 200\,\text{GeV}$ (upper curve, gold) and $\sqrt{s} = 5.5\,\text{TeV}$ (two bottom curves, lead). The bottom dashed curve includes only the effects of $\bar{b}b$ dipole breakup and high-twist shadowing of beauty production; the solid curve is corrected for gluon shadowing.

former case the "frozen" approximation is not well justified at $y = 0$, where $t_c \sim 4\,\text{fm}$.

B. Leading twist gluon shadowing

In terms of the Fock decomposition gluon shadowing for $\bar{c}c$ production is associated with higher Fock states $|\bar{c}cg\rangle$, etc. First, one should evaluate the kinematic condition for gluon shadowing, $t_c^{\bar{c}cg} \gtrsim R_A$, where $t_c^{\bar{c}cg}$ is the coherence time or the lifetime of a $\bar{c}cg$ fluctuation in a gluon. This time can be related to the Ioffe time as

$$t_c^{\bar{c}cg} = \frac{P_g}{x m_N}, \tag{13}$$

where the factor $P_g \approx 0.1$ was evaluated in Ref. [11] and found to be scale independent. Its smallness is caused by the large intrinsic transverse momenta of gluons in hadrons, supported by numerous evidences in data [12,13]. Thus, shadowing for gluons onsets at $x \lesssim 0.01$, which is a smaller x value than for quarks. As the result, no gluon shadowing is possible for charmonium production in any of fixed-target experiments performed so far [3,14].

Even at the energy $\sqrt{s} = 200\,\text{GeV}$ the values of x_2 defined in Eq. (2) are too large for gluon shadowing, $0.024 > x_2 > 0.0033$, within the measured rapidity interval $0 < y < 2$. We rely upon the next to leading order (NLO) analysis [15] of deeply inelastic scattering (DIS) data, which suggests a very weak gluon shadowing, as is depicted in Fig. 6 in Ref. [15]. Such a weak shadowing is in good agreement with the theoretical predictions [12]. The nuclear ratio presented by the dashed curve in Fig. 2 corrected for gluons shadowing at $Q^2 = 10\,\text{GeV}^2$ (see Fig. 6 in Ref. [15]), is depicted by a solid curve. We see that the effect of gluon shadowing is indeed vanishingly small. Even at the energy of the LHC, $\sqrt{s} = 5.5\,\text{TeV}$ and $y = 0$, gluon shadowing according to Refs. [12,15] is extremely small, only 3% at $x_2 = 5.5 \times 10^{-3}$, and will be neglected in what follows.

Apparently, for Υ production gluon shadowing is weaker than for charmonia. No gluon shadowing affects Υ production at the energies of the RHIC, as depicted by the upper curve in Fig. 4, since the values of x_2 are too large. The effect of gluon shadowing at the energy of the LHC is visible, and the full calculation is shown by the bottom solid curve. It was calculated using the gluon parton distribution function (PDF) of [15] at $Q^2 = 100\,\text{GeV}^2$.

III. TRANSITION FROM pA to AA

At fist glance one might extrapolate the nuclear effects from pA to AA collisions in a straightforward way: $R_{AA}(\vec{b}, \vec{\tau}) = R_{pA}(\vec{\tau}) \times R_{pA}(\vec{b} - \vec{\tau})$, where $\vec{b}$ is the impact parameter of nuclear collisions and J/Ψ is produced at impact parameter $\vec{\tau}$. Indeed, such a "data-driven" procedure was used in Refs. [10,16] to predict the cold nuclear matter effects in nuclear collisions based on the measurements of b dependence of nuclear suppression in pA. There are several reasons, however, that make such a transition model dependent.

A. Double-color filtering

As we have discussed, the survival probability of a $\bar{c}c$ dipole propagating through a nucleus is subject to color transparency. This effect in AA collisions turns out to be nonfactorizable. This can be illustrated by the following example. Let a $\bar{c}c$ dipole of transverse separation r_T propagate through a slice of nuclear medium of thickness T_A with survival probability $S_{pA}(r_T) = \exp(-C\, r_T^2\, T_A)$. To clarify the appearance of the effect we rely on the simplified size distribution function $W(r_T) \propto \exp[-r_T^2/\langle r_T^2\rangle]$ adjusted to the distribution (5) with $\langle r_T^2\rangle = 0.045\,\text{fm}^2$. Then the nuclear attenuation factor takes the form

$$S_{pA} = \int d^2 r_T\, W(r_T)\, S_{pA}(r_T) = \frac{1}{1 + C\langle r_T^2\rangle\, T_A}. \tag{14}$$

Naively, one could expect $S_{AA}(b) = S_{pA}^2$. Such a factorization is valid only in the dipole representation for a given dipole size, $S_{AA}(r_T) = S_{pA}^2(r_T) = \exp(-2 \times C r_T^2 T_A)$. Factor 2 is introduced because the dipole is simultaneously attenuated by both nuclei. Now we can repeat our averaging over dipole size and compare the result (left) with the conventional recipe (right):

$$S_{AA} = \frac{1}{1 + 2\, C\langle r_T^2\rangle\, T_A} \;\Leftrightarrow\; \frac{1}{\left[1 + C\langle r_T^2\rangle\, T_A\right]^2}. \tag{15}$$

We see that the two absorption factors are quite different, especially for $C\langle r_T^2\rangle T_A \gtrsim 1$. The source of the difference is color filtering. Namely, the mean transverse size of a $\bar{c}c$ wave packet propagating through a nucleus is getting smaller, since large-size dipoles are filtered out (absorbed) with a larger probability [17,18]. Such a dipole with a reduced mean size penetrates more easily through the second colliding nucleus, compared with a pA collision. The mutual color filtering makes both nuclei more transparent.

Now we are in a position to perform realistic calculations for the nuclear suppression factor in AB collisions. Provided

that the $\bar{c}c$ production occurs in the long coherence length regime for both nuclei, the nuclear suppression factor at impact parameter b reads

$$R_{AB}(b) = \frac{1}{T_{AB}(b)} \int d^2\tau \, \frac{T_A(\tau) T_B((\vec{b}-\vec{\tau})}{(\Lambda_A^+ - \Lambda_A^-)(\Lambda_B^+ - \Lambda_B^-)} \times \ln\left[\frac{(1+\Lambda_A^- + \Lambda_B^+)(1+\Lambda_A^+ + \Lambda_B^-)}{(1+\Lambda_A^+ + \Lambda_B^+)(1+\Lambda_A^- + \Lambda_B^-)}\right]. \quad (16)$$

where

$$\Lambda_A^+ = \frac{\langle r_T^2 \rangle}{2} C\left(E_{\bar{c}c}^A\right) T_A(\tau), \quad (17)$$

$$\Lambda_A^- = \frac{7\langle r_T^2 \rangle}{32} C\left(E_{\bar{c}c}^A\right) T_A(\tau), \quad (18)$$

$$\Lambda_B^+ = \frac{\langle r_T^2 \rangle}{2} C\left(E_{\bar{c}c}^B\right) T_B(\vec{b}-\vec{\tau}), \quad (19)$$

$$\Lambda_B^- = \frac{7\langle r_T^2 \rangle}{32} C\left(E_{\bar{c}c}^B\right) T_B(\vec{b}-\vec{\tau}), \quad (20)$$

and $E_{\bar{c}c}^{A,B}$ are the energies of the $\bar{c}c$ in the rest frames of the nuclei A and B, respectively. The result of Eq. (16) is plotted as the upper solid curve in Fig. 5.

For comparison, the result of conventional calculations assuming simple multiplication of the suppression factors in the two nuclei is depicted by the dashed curve. We see that the mutual color filtering makes the nuclei considerably more transparent. This effect should be more prominent for production of Ψ' and χ.

With Eq. (16) we can trace the y dependence of R_{AA}. It turns out to be rather weak at the energy of the RHIC, due to the approximate linearity of y dependence in pA depicted in Fig. 2, which leads to a compensation of the nuclear effects in the colliding nuclei. However, at sufficiently large y, say, $y = 2$, the condition of long coherence length breaks down in one of the nuclei. Then the $\bar{c}c$ dipole size is not frozen by Lorentz time delation, and the filtering in this particular nucleus is not effective any more. In this case the conventional multiplicative procedure is applicable, but the suppression factor in one nucleus (high $E_{\bar{c}c}$) should be calculated differently, for a short t_c regime. The result of such calculation is plotted by the bottom solid curve in Fig. 3. We see that the nuclear suppression at $y = 2$ is stronger than at $y = 0$. This happens due to disappearance of the double-color filtering effect.

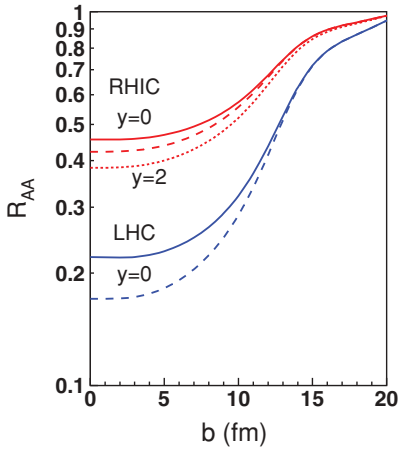

FIG. 5. (Color online) Effects of double-color filtering. J/Ψ suppression by ISI effects in Au-Au collisions at $\sqrt{s} = 200\,\text{GeV}$ as a function of b. The upper and bottom pairs of curves (solid and dashed) correspond to $y = 0$ and energies $\sqrt{s} = 200\,\text{GeV}$ and 5.5 TeV, respectively. Solid and dashed curves present the results at $y = 0$ including and excluding the effect of double-color filtering, respectively. The dotted curve demonstrates rapidity dependence of the ISI effects at RHIC. It is calculated at $y = 2$ and is to be compared with the upper solid curve at $y = 0$.

B. Boosting the saturation scale in AA collisions

Another mechanism that violates the conventional multiplicative procedure for the transition from pA to AA collisions is the mutual boosting of the saturation scale in the colliding nuclei. It is controlled by the following reciprocity equations [19]:

$$\tilde{Q}_{sB}^2(x_B) = \frac{3\pi^2}{2}\alpha_s\left(\tilde{Q}_{sA}^2 + Q_0^2\right) x_B g_N\left(x_B, \tilde{Q}_{sA}^2 + Q_0^2\right) T_B, \quad (21)$$

$$\tilde{Q}_{sA}^2(x_A) = \frac{3\pi^2}{2}\alpha_s\left(\tilde{Q}_{sB}^2 + Q_0^2\right) x_A g_N\left(x_A, \tilde{Q}_{sB}^2 + Q_0^2\right) T_A, \quad (22)$$

where we consider a collision of two rows of nucleons T_A and T_B, and production of a heavy quark pair with fractional momenta x_A and x_B relative to the colliding nucleons. In what follows we consider heavy quarkonium production at forward rapidities relative to the momentum direction of nucleus A, which we call the beam. Correspondingly, the target nucleus is B. The values of $x_{A(B)}$ in Eqs. (21) and (22) for charmonium production with positive rapidity y are calculated as

$$x_{A(B)} = \frac{\sqrt{M_{J/\Psi}^2 + \langle p_T^2 \rangle}}{\sqrt{s}} e^{\pm y}. \quad (23)$$

The mean transverse momentum squared of J/Ψ produced in pp collisions at the energies of RHIC and LHC are $\langle p_T^2 \rangle \approx 4\,\text{GeV}^2$ and $7\,\text{GeV}^2$, respectively.

The gluon distribution function $g_N(x, Q^2)$ contains the parameter Q_0 needed to regularize the infrared behavior adjusting the saturation momentum in a pA collision to the known value [20]:

$$Q_{sA}^2(b, E_{\bar{Q}Q}) = \vec{\nabla}_{r_T}^2 \, \sigma_{\text{dip}}(r_T, E_{\bar{Q}Q})|_{r_T=0} \, T_A(b) = 2C(E_{\bar{Q}Q})\, T_A(b), \quad (24)$$

where parameter $C(E_{\bar{Q}Q})$ introduced in Eq. (3) is well fixed by HERA data. Solution of Eq. (24) leads to the infrared cutoff parameter $Q_0^2 \approx 1.7\,\text{GeV}^2$, which is nearly independent of energy.

Solution of Eqs. (21) and (22) shows that the modified saturation scales $\tilde{Q}_{sA(B)}^2$ in AB collisions considerably exceed the conventional scales (24) relevant for pA collisions. The essential point of this consideration is that the boosted saturation scale leads to an increase of the breakup cross section of a dipole, because the saturation momentum is directly related to the factor $C(E)$ in the dipole cross section (24).

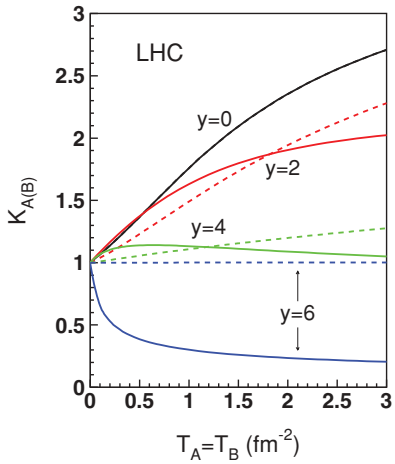

FIG. 6. (Color online) The boosting factors $K_A(x_A)$ (solid curves) and $K_B(x_B)$ (dashed curves) defined in Eq. (26) and calculated with the reciprocity equations (21) and (22) for $\sqrt{s} = 5.5$ TeV with $x_{A(B)}$ defined in Eq. (23). Each pair of curves is marked by the rapidity for which it is calculated.

Thus, the breakup cross section $\sigma_{\rm dip}(r_T)$ for a dipole propagating through the nucleus B modifies as

$$\sigma_{\rm dip}(r_T) \Rightarrow \tilde{\sigma}^B_{\rm dip}(r_T) = K_A\, \sigma_{\rm dip}(r_T), \tag{25}$$

where

$$K_A = \frac{\tilde{Q}^2_{sA}}{Q^2_{sA}}. \tag{26}$$

This boosting factor for the dipole absorption cross section in the nucleus B is controlled by the boosted saturation scale of the nucleus A, which implicitly depends on T_A, T_B, x_A, and x_B in accordance with Eqs. (21) and (22). Correspondingly the boosted breakup cross section of the $\bar{c}c$ dipole propagating through the nucleus A is given by $\tilde{\sigma}^A_{\rm dip}(r_T) = K_B\, \sigma_{\rm dip}(r_T)$.

We calculated the factors K_A and K_B solving the reciprocity equations (21) and (22) supplied with the MSTW2008 code [21] for the gluon distributions. The results at $\sqrt{s} = 5.5$ TeV are plotted in Fig. 6 as a function of $T_A = T_B$ (central AA collision) for different rapidities of the produced charmonium. Solid and dashed curves present K_A and K_B, respectively.

We see that the boosting factors are maximal at $y = 0$, where $K_A \equiv K_B$. At forward rapidities x_A rises, while x_B decreases. As a result, the boosting factors K_A and K_B remain similar, and both are falling with rapidity. Eventually, at large rapidity $y = 6$ the projectile x_A becomes so large that the shift of the scale does not lead to an increase of the gluons density in A but makes it smaller [22]. Therefore the effect of boosting turns into a suppression, i.e., the nucleus A in this case becomes more transparent, rather than opaque, for J/Ψ. Similar calculations at $\sqrt{s} = 200$ GeV depicted in Fig. 7 demonstrate different behavior.

Surprisingly, while K_B is falling with rapidity, as expected, K_A is rising. This rise of the boosting factor is related to a steep drop at forward rapidities of the saturation momentum in the projectile nucleus A, the denominator of Eq. (26). In fact, the very existence of a saturation regime at such large x_Q is questionable.

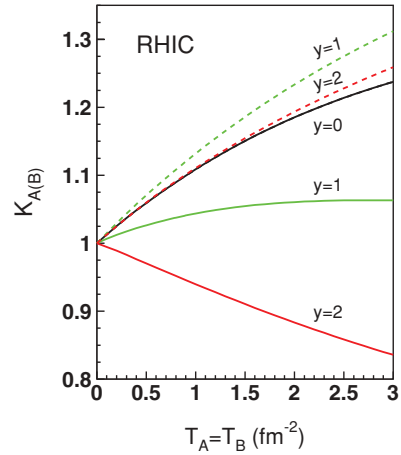

FIG. 7. (Color online) The same as in Fig. 6, but at $\sqrt{s} = 200$ GeV.

We see that the boosting effect significantly increases the saturation scales in colliding heavy nuclei, especially at the midrapiditiy and high energies. The rapidity dependence of the boosting factor is more complicated and is related to different variation with scale of the gluon distribution function at different values of Bjorken x. It is worth remembering that what is plotted in Figs. 6 and 7 are the ratios. The absolute value of the saturation momentum in the nucleus B (A) is steeply rising (falling) with rapidity.

The transparency of the nuclear medium for heavy-quark dipoles in the case of nuclear collisions is different from what is measured in pA collisions. The simplified prescription of Refs. [2,10,16] for the transition pA to AA may be quite incorrect.

In Fig. 8 we demonstrate the strength of the boosting effect on the production rate of J/Ψ in the central ($b = 0$) Au-Au collision as a function of impact parameter τ.

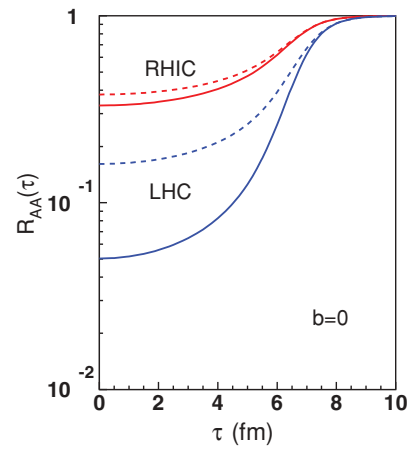

FIG. 8. (Color online) Effect of the boosted saturation scale on the nuclear ratio for J/Ψ production in central ($b = 0$) Au-Au collisions at $y = 0$ as a function of impact parameter τ. The upper and bottom dashed curves correspond to $\sqrt{s} = 200$ GeV and 5.5 TeV, respectively. They are calculated in the same way as the solid curves in Fig. 5. The solid curves here are calculated with the boosted saturation scale, which makes the nuclei more opaque for heavy dipoles.

The dashed curves include the double-color filtering effect but exclude the saturation scale boosting, which is added to produce the solid curves. The solid curves include the effect of boosted saturation scale. The upper and bottom pairs of curves correspond to the energies of the RHIC and LHC, respectively. We conclude that J/Ψ should be significantly stronger suppressed in AA collisions, more than usually expected extrapolating from pA, and one should not misinterpret this suppression as an anomalous effect related to FSI with the dense medium. Notice that a stronger suppression of J/Ψ in the ISI stage of the collision compared to the one used in Ref. [2] should result in an even smaller transport coefficient of the dense medium extracted from RHIC data on J/Ψ production.

C. Boosted gluon shadowing

As we have already mentioned, in terms of the Fock decomposition gluon shadowing corresponds to multiple interactions of higher Fock states, containing gluons. One may wonder if the double-color filtering effect can affect the amount of gluon shadowing in nuclear collisions. The answer is no. The lifetime of such a fluctuation produced by a nucleon in the nucleus A may be sufficiently long only relative to the nucleus B but is very short relative to the parent nucleus A. Therefore no gluonic fluctuations undergo double-color filtering. In terms of Gribov inelastic shadowing this means that the diffractive excitation of the nucleons of A propagate through B independently of the excitations of B propagating through A.

Thus, the gluon shadowing factors factorize in AB collisions:

$$R_g^{AB}(\vec{b},\vec{\tau}) = R_g^A(\tau)\, R_g^B(\vec{b}-\vec{\tau}). \tag{27}$$

Even if gluon shadowing for heavy quarkonium production in pA collision is known, say, from analyses of DIS data [15], it is integrated over the impact parameter, while in Eq. (27) one needs to know its impact parameter dependence in order to predict gluon shadowing in heavy ion collisions. This problem is already a serious obstacle for extrapolation from pA to AA.

Aside from the ad hoc parametrizations of the b dependence existing in the literature, one has to rely on a fully developed theoretical model for gluon shadowing to predict its b dependence. Unfortunately, no satisfactory theoretical description, which would work at all kinematic regimes, has been developed so far. The most rigorous quantum-mechanical treatment of gluon shadowing within the path-integral technique [12,23] is the lowest order calculation, which might be a reasonable approximation only for light nuclei, or for the onset of shadowing. Contribution of higher Fock components is still a challenge. This problem has been solved only in the limit of long coherence lengths for all radiated gluons, in the form known as the Balitsky-Kovchegov equation (BK) [24,25]. Numerical solution of this equation is quite complicated and includes a lot of modeling [26]. A simpler equation, which employs only a modeled shape of the saturated gluon distribution, was derived in Ref. [22]. It leads to a gluon distribution in nuclei, which satisfies the unitarity bound [27], and is quite similar to the numerical solutions of the BK equation. The equation reads [22]

$$R_g = 1 - \frac{R_g^2\, n_0^2\, n_{\rm eff}}{(1+R_g\, n_0)^2(1+n_{\rm eff})}, \tag{28}$$

where

$$\begin{aligned} n_0(E_{\bar{c}c},b) &= \frac{9\,C(E_{\bar{c}c})}{2\,Q_{qN}^2(E_{\bar{c}c})}\,T_A(b), \\ n_{\rm eff}(E_{\bar{c}c},b) &= \frac{9}{4}\,C(E_{\bar{c}c})\,r_0^2\,T_A(b). \end{aligned} \tag{29}$$

The energy-dependent factor $C(E_{\bar{c}c})$ was introduced in Eq. (3). The mean size of a gluonic dipole, $r_0 \approx 0.3$ fm, is dictated by data [12,13]. We rely on the saturated shape of the dipole-nucleon cross section with the saturation scale $Q_{qN}(E_{\bar{c}c}) = 0.19\,\text{GeV} \times (E_{\bar{c}c}/1GeV)^{0.14}$, fitted to DIS data [12,22]. One can switch from energy to Bjorken x dependence in these equations, using the relation (23) and replacing $s \Rightarrow 2E_{\bar{c}c}m_N$.

Notice that Eq. (28) does not contain any hard scale, but only a semihard one controlled by r_0 [13]. Therefore its solution should be treated as the starting gluon distribution at the semihard scale ($Q^2 \approx 4/r_0^2 \approx Q)^2$, where Q_0 was introduced in Eqs. (21) and (22). Shadowing for heavy quarkonium production should be Dokshitzer-Gribov-Lipatov-Altarelli-Parisi (DGLAP) evolved up to an appropriate hard scale.

The effect of boosted saturation scale leads to a modification of the factor $C(E_{\bar{c}c})$, which is different for nuclei A and B:

$$C(E_{\bar{c}c}) \Rightarrow \tilde{C}_{A(B)}(E_{\bar{c}c}) = K_{A(B)}\,C(E_{\bar{c}c}). \tag{30}$$

Solving Eq. (28) with such a boosted saturation scale, one arrives at a modified nuclear ratio for gluons in nuclei A and

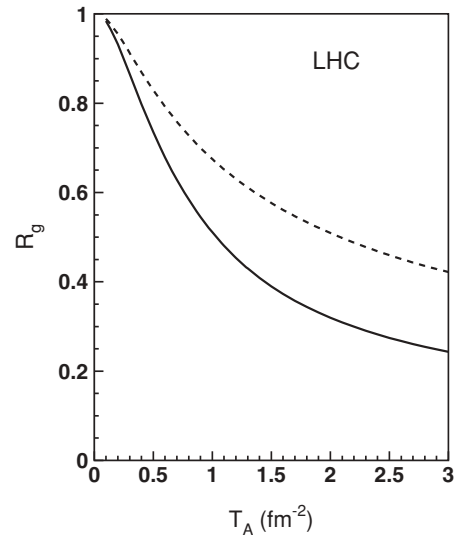

FIG. 9. Gluon nuclear ratio R_g as function of nuclear thickness T_A calculated with Eq. (28) at the semihard scale Q_0. The dashed curve presents gluon shadowing corresponding to hadron-nucleus collisions. The solid curve includes the boosting effects specific for central nucleus-nucleus collisions ($T_A = T_B$). Shadowing is calculated at the starting scale Q_0 and should be evolved up to a higher scale.

B, $\tilde{R}_g^{A(B)}(E_{\bar{c}c}, b)$, for which the factorized relation (27) can be used:

$$\tilde{R}_g^{AB}(\vec{b}, \vec{\tau}) = \tilde{R}_g^{A}(\tau)\, \tilde{R}_g^{B}(\vec{b} - \vec{\tau}). \tag{31}$$

A numerical example for the boosting effect on gluon shadowing is depicted in Fig. 9.

The dashed and solid curves show the solutions of Eq. (28) without and with inclusion of the boosting effects, calculated for J/Ψ produced with $y = 0$ at $\sqrt{s} = 5500\,\text{GeV}$. We see that the boosting effect is considerable. As was mentioned, shadowing is calculated at the starting scale Q_0 and should be evolved up to a proper higher scale.

IV. SUMMARY AND PROSPECTIVES

The dipole formalism based in the universal dipole cross section well fitted to HERA data successfully describes the propagation of heavy quark dipoles through cold nuclear matter. Our parameter-free calculation presented in Fig. 2 agrees well with data from the RHIC for J/Ψ production in d-Au collisions. We do all calculations within the "frozen" approximation, assuming that the dipole size does not fluctuate during propagation through the nucleus. This condition is satisfied provided that the coherence time is long, $t_c \gg R_A$, which is well justified at the energies of the RHIC and LHC.

We identify the main source of the observed nuclear suppression as a combined effect of breakup of the produced $\bar{c}c$ dipole in nuclear medium and charm quark shadowing. Although both are the high twist effects, their contribution to the observed nuclear suppression considerably exceeds the effect of leading twist gluon shadowing. The latter is expected to be rather weak, basing on either theoretical predictions [12] or the NLO analysis [15] of DIS data.

Even if the nuclear effects for heavy quarkonium production are understood, the transition to AA collisions is rather complicated. Several new phenomena, specific for nuclear collisions, make such a transition model dependent. The first, double-color filtering, makes the nuclei more transparent for quark dipoles than in pA collisions. The second is the mutual boosting of the saturation scales in the colliding nuclei, which makes the nuclei more opaque for quark dipoles. Although these two effects act in opposite directions, the latter is much stronger, as can be seen in Fig. 8.

Another direct consequence of the increased saturation scale in nuclear collisions is the boosting of gluon shadowing, which violates the factorized relation, Eq. (27).

A direct way to access the saturation scale experimentally is to measure transverse momentum broadening of charmonia produced on nuclei. Then the boosting effect should show up as an increase of broadening of J/Ψ produced in AA compared to pA collisions. Indeed, such an effect was clearly observed in the NA60 and NA50 experiments at $E_{\text{lab}} = 158\,\text{GeV}$ [28]. The broadening in nuclear collisions was found to be twice as large as in pA measurements with the same path length in the nuclear medium. Within the rather good statistical and systematic accuracy, the effect is quite certain. The magnitude of the observed boosting is larger than is predicted by Eqs. (21) and (22) at this energy, so this problem needs further study, and the data are to be confirmed by independent measurements.

Although we considered here only the high-energy limit of "frozen" dipoles, the pA to AA transition is not trivial at medium high energies, say, at SPS, either [3]. This case will be also investigated and published elsewhere.

ACKNOWLEDGMENTS

We are thankful to Sasha Tarasov for numerous informative discussions. This work was supported in part by Fondecyt (Chile) Grants No. 1090291, 1090236, and 1100287, by DFG (Germany) Grant No. PI182/3-1, and by Conicyt-DFG Grant No. 084-2009.

[1] T. Matsui and H. Satz, Phys. Lett. B **178**, 416 (1986).
[2] B. Z. Kopeliovich, I. K. Potashnikova, and I. Schmidt, Phys. Rev. C **82**, 024901 (2010).
[3] B. Z. Kopeliovich, arXiv:1007.4513 [hep-ph].
[4] B. Kopeliovich, A. Tarasov, and J. Hüfner, Nucl. Phys. A **696**, 669 (2001).
[5] S. J. Brodsky and J. P. Lansberg, Phys. Rev. D **81**, 051502 (2010).
[6] D. Kharzeev, E. Levin, M. Nardi, and K. Tuchin, Nucl. Phys. A **826**, 230 (2009).
[7] K. J. Golec-Biernat and M. Wusthoff, Phys. Rev. D **60**, 114023 (1999).
[8] B. Z. Kopeliovich and B. G. Zakharov, Phys. Rev. D **44**, 3466 (1991).
[9] H. de Vries, C. W. de Jager, and C. de Vries, At. Nucl. Nucl. Data Tabl. **36**, 495 (1987).
[10] A. Adare *et al.* (PHENIX Coll.), Phys. Rev. C **77**, 024912 (2008).
[11] B. Z. Kopeliovich, J. Raufeisen, and A. V. Tarasov, Phys. Rev. C **62**, 035204 (2000).
[12] B. Z. Kopeliovich, A. Schäfer, and A. V. Tarasov, Phys. Rev. D **62**, 054022 (2000).
[13] B. Z. Kopeliovich, I. K. Potashnikova, B. Povh, and I. Schmidt, Phys. Rev. D **76**, 094020 (2007).
[14] B. Z. Kopeliovich, J. Nemchik, I. K. Potashnikova, M. B. Johnson, and I. Schmidt, Phys. Rev. C **72**, 054606 (2005).
[15] D. de Florian and R. Sassot, Phys. Rev. D **69**, 074028 (2004).
[16] R. Granier de Cassagnac, J. Phys. G **34**, S955 (2007).
[17] B. Z. Kopeliovich, L. I. Lapidus, and A. B. Zamolodchikov, JETP Lett. **33**, 595 (1981); Pisma Zh. Eksp. Teor. Fiz. **33**, 612 (1981).
[18] G. Bertsch, S. J. Brodsky, A. S. Goldhaber, and J. G. Gunion, Phys. Rev. Lett. **47**, 297 (1981).
[19] B. Z. Kopeliovich, H. J. Pirner, I. K. Potashnikova, and I. Schmidt, arXiv:1007.1913 [hep-ph].
[20] M. B. Johnson, B. Z. Kopeliovich, and A. V. Tarasov, Phys. Rev. C **63**, 035203 (2001).
[21] A. D. Martin, W. J. Stirling, R. S. Thorne, and G. Watt, Eur. Phys. J. C **63**, 189 (2009); **64**, 653 (2009).

[22] B. Z. Kopeliovich, I. K. Potashnikova, and I. Schmidt, Phys. Rev. C **81**, 035204 (2010).
[23] B. Z. Kopeliovich, J. Raufeisen, A. V. Tarasov, and M. B. Johnson, Phys. Rev. C **67**, 014903 (2003).
[24] I. Balitsky, Nucl. Phys. B **463**, 99 (1996).
[25] Y. V. Kovchegov, Phys. Rev. D **60**, 034008 (1999).
[26] J. L. Albacete, N. Armesto, J. G. Milhano, C. A. Salgado, and U. A. Wiedemann, Phys. Rev. D **71**, 014003 (2005).
[27] B. Z. Kopeliovich, E. Levin, I. K. Potashnikova, and I. Schmidt, Phys. Rev. C **79**, 064906 (2009).
[28] E. Scomparin (NA60 Coll.), Nucl. Phys. A **830**, 239C (2009); R. Arnaldi (NA60 Coll.), *ibid.* **830**, 345C (2009).